Conf-821049--15

INFLUENCE OF HELIUM-INJECTION SCHEDULE AND PRIOR THERMOMECHANICAL TREATMENT ON THE MICROSTRUCTURE OF TYPE 316 SS*

A. Kohyama+, G. Ayrault and A.P.L. Turner
Materials Science and Technology Division
Argonne National Laboratory
Argonne, Illinois 60439

CONF-821049--15

DE83 007822

DISCLAIMER

This report was prepared as an account of work sponsored by an agency of the United States Government. Neither the United States Government nor any agency thereof, nor any of their employees, makes any warranty, express or implied, or assumes any legal liability or responsibility for the accuracy, completeness, or usefulness of any information, apparatus, product, or process disclosed, or represents that its use would not infringe privately owned rights. Reference herein to any specific commercial product, process, or service by trade name, trademark, manufacturer, or otherwise does not necessarily constitute or imply its endorsement, recommendation, or favoring by the United States Government or any agency thereof. The views and opinions of authors expressed herein do not necessarily state or reflect those of the United States Government or any agency thereof.

October 1982

The submitted manuscript has been authored by a contractor of the U. S. Government under contract No. W-31-109-ENG-38. Accordingly, the U. S. Government retains a nonexclusive, royalty-free license to publish or reproduce the published form of this contribution, or allow others to do so, for U. S. Government purposes.

To be presented at the Fall Meeting of TMS-AIME, St. Louis, MO., October 25-28, 1982. Proceedings to be published in the Journal of Nuclear Materials.

*Work supported by the U. S. Department of Energy and US-Japan fusion cooperation program.

+On leave from Department of Materials Science, University of Tokyo, Hongo, Bunkyo-ku, Tokyo 113, Japan.

MASTER

DISTRIBUTION OF THIS DOCUMENT IS UNLIMITED

INFLUENCE OF HELIUM INJECTION SCHEDULE AND PRIOR THERMOMECHANICAL TREATMENT ON THE MICROSTRUCTURE OF TYPE 316 SS*

A. Kohyama+, G. Ayrault and A.P.L. Turner
Materials Science and Technology Division
Argonne National Laboratory
Argonne, Illinois 60439

SUMMARY

The influence of different helium-injection scheudles on microstructure development in Ni^+ ion irradiated 316 SS at 625 C is discussed. Injection schedules were chosen to (1) approximate the MFR condition and (2) mimic the mixed-spectrum reactor condition. Dual-ion irradiation to 25 dpa produced strongly bimodal cavity size distributions in solution-annealed and solution-annealed and aged samples, whereas single-ion irradiation followed by dual-ion irradiation to the same dose produced a cavity size distribution with a substantial component of intermediate-size cavities. Dual-ion irradiation produced only very small cavities in 20% CW material, while single-ion followed by dual-ion irradiation produced some intermediate size cavities and greater swelling.

INTRODUCTION

A major problem impacting upon the adaptability of candidate alloys as structural materials in D-T magnetic fusion reactors (MFR) is the influence of transmutant gases on the microstructural development during irradiation, and hence on mechanical properties. Helium and hydrogen will be the most abundant gaseous transmutation products in MFR, and of these helium is thought to pose

*Work supported by the U. S. Department of Energy and US-Japan fusion cooperation program.

+On leave from Department of Materials Science, University of Tokyo, Hongo, Bunkyo-ku, Tokyo 113, Japan.

the greater problem because of its low solubility in metals.

Since no operating fusion reactors or intense fusion-spectrum neutron sources exist at present, studies of helium effects rely upon simulation of the MFR environment. Mixed-spectrum reactor irradiation is commonly used for study of helium effects on radiation damage in nickel-bearing alloys. In this case, helium is generated via the two step reaction

$$^{58}Ni(n,\gamma)^{59}Ni,\ ^{59}Ni(n,\alpha)^{56}Fe$$

At sufficient neutron doses, the ^{59}Ni concentration in austenitic alloys can reach levels where the helium generation rate reaches or exceeds the high level expected in MFR (~15 appm He/dpa). However, during the earliest phase of microstructure nucleation at the start of irradiation in mixed spectrum reactors there is no helium generation because no ^{59}Ni has been produced. In contrast, MFR neutrons will generate helium rapidly even at the lowest doses. In this study we have dual-ion irradiated 316 SS samples using helium injection schedules intended to (1) approximate the MFR condition of steady helium generation, and (2) mimic the mixed-spectrum reactor condition of rapid helium production at high dose and no helium production at low dose.

MATERIALS AND PROCEDURE

The material for this study was 316 SS from the MFE heat (15893). Irradiations under all of the conditions that are described below were performed on samples with three prior thermomechanical treatments: solution annealed (0.5 h at 1050 C), solution annealed and aged (1 h at 1050 C, 10 h at 800 C) and 20% cold worked. The irradiations were performed at 625 C, which is near the peak swelling temperature for the damage rate of 3×10^{-3} dpa/sec

that was employed in the study. Nickel ion irradiation (3.0 MeV Ni^+) was used for damage production. The simultaneous helium injections were performed with degraded 0.83 MeV He^+ ions [1].

Samples were irradiated with four dose/helium histories. For simplicity, each of these histories is assigned a discriptive code (e.g. 5S for (1) below), which is listed with each dose/helium history. The histories were:

(1) single-ion irradiation to 5 dpa (5S),

(2) dual-ion irradiation to 5 dpa with 15 appm He/dpa (5D),

(3) single-ion irradiation to 5 dpa followed by 20 dpa of dual-ion irradiation with 18.8 appm He/dpa to give the same final helium concentration as (4) (25SD), and

(4) dual-ion irradiation to 25 dpa with 15 appm He/dpa (25D).

Histories 3 and 4 (25SD and 25D) are intended to mimic mixed spectrum reactor and MFR irradiation, respectively. Histories 1 and 2 (5S and 5D) provide information on the microstructures that the 25 dpa samples (25SD and 25D) had at low dose. A summary of the irradiation conditions is presented in Table 1.

TEM observations of irradiated samples were performed using the JEM-100CX electron microscope. The carbon spot method [2] was used to measure the foil thickness of the observed microstructures, and the cavity size distributions were obtained from observations of photo micrographs with a Zeiss particle size analyzer. In all cases the micrographs for microstructure analyses were recorded in a (200) two beam diffraction condition for dislocation contrast or were recorded in underfocused absorption contrast to image the cavities.

EXPERIMENTAL RESULTS

Typical microstructures for 5S, 5D, 25SD and 25D samples (histories 1,2,3, and 4, respectively) are prsented in Figs. 1-2. Figure 1 shows solution annealed (SA) samples; figure 2 shows solution annealed and aged (SAA) samples; figure 3 shows 20% cold worked (CW) samples. In all cases the microstructures are recorded in a (200) two-beam diffraction condition for dislocation contrast or in underfocused adsorption contrast to image the cavities.

The microstructures in 5 dpa solution annealed samples 5S and 5D, Fig. 1, are quite different from one another. No visible cavities are present in the single-ion samples, whereas dual-ion irradiation produced significant cavity nucleation and growth. Dislocation structures in both 5S and 5D samples consist almost entirely of Frank loops, but the loop number density was higher and the loop size smaller in the 5D sample. Clearly the helium played a major role in nucleation of both cavities and loops. At 25 dpa the 25SD and 25D samples have similar dislocation microstructures consisting of both loops and lines. Although the dislocation structure appears to have recovered at 25 dpa from differences present at 5 dpa, the difference in the cavity microstructure persists. The cavity size distribution in the 25D sample was clearly bimodal in nature but the size distribution of 25SD was not as strongly bimodal as in the 25D samples.

Microstructure development in solution annealed and aged material, Fig. 2, closely paralleled that in solution annealed samples. Again no cavities were present in the 5S sample and the loop density was low, while cavity growth was well under way in the 5D sample and higher number densities of smaller loops were present. Also the 25D beam history produced a strongly bimodal cavity size distribution, whereas cavities of intermediate size were profuse follow-

ing 25SD irradiation, as in SA material.

In 20% cold worked material the dislocation densities were high for all beam histories and swelling was low, as expected. The 5 dpa samples 5S and 5D, Fig. 3, looked nearly identical to one another, except that a few very small (barely resolvable) cavities were seen in the 5D sample. At 25 dpa the 25D sample contained no cavities larger than 8 nm. Small cavities were profuse and most, if not all, were associated with dislocations. The 25SD history produced, in addition to the high number density of small cavities, a very low number density of cavities as large as 15 nm.

The dislocation structures in SA or SAA samples irradiated to 5 dpa, i.e., 5S and 5D, were predominantly of the Frank loop type with a slight difference in the number density of loops between 5S and 5D. The average diameter of Frank loops in SA materials was larger than in SAA materials. At damage levels between 5 dpa and 15 dpa, unfaulting of the Frank loops occurred with glide and climb of dislocations to form a tangled dislocation network. This unfaulting of Frank loops led to saturation of the dislocation densities at about 10 dpa in SA and SAA materials.

The most notable difference between SA and SAA samples was the low dose dislocation microstructure. Loop number densities were lower and loop diameters larger in SA samples than in SAA specimens at 5 dpa after both single- and dual-ion irradiation. In 20% cold worked (CW) samples, substantial recovery of the as-prepared dislocation density occurred initially (< 5 dpa) and then the irradiation-produced dislocation density increased to the saturation value. These results were similar to the results obtained for molybdenum alloys [3] and 316 SS [4] during in-situ irradiation in HVEM. The dependence of dislocation density in these specimens on irradiation damage dose is shown in Fig. 4.

Radiation induced needle-like precipitates were present in all of the irradiated samples. In SA and SAA materials irradiated to 5 dpa, the needle-like precipitates exhibited a preferential orientation in the <100> direction. The precipitates in 5D specimens were more highly aligned than those in 5S specimens. The number density of precipitates in 5S materials was higher than in the 5D material. In SA and SAA materials irradiated to 25 dpa, the precipitate number density was not significantly different between the 25SD and 25D irradiation schedules. Both the grain boundary precipitates and the needle-like precipitates in SAA material were larger than in SA material. The needle-like precipitates were poorly aligned in the SAA material compared to the SA material. In CW material, many needle-like precipitates that were smaller than in SA and SAA materials could be observed. The precipitates in CW materials did not appear to be well aligned and the number density of the precipitates was very low.

The cavity size distribution in the solution annealed (25D) specimen (Fig. 5) was clearly bimodal in nature with a high number density of small cavities (< 8 nm) and a lower number density of large cavities (up to 40 nm). The 25SD specimen contained a high number density of small cavities and the maximum cavity size was similar to that in the 25D sample. However, the size distribution in the 25SD specimen was not as strongly bimodal as in the 25D samples; there were many cavities in the 8 to 30 nm size range.

Cavity microstructure development in the SAA material (Fig. 6) closely paralleled their development in SA specimens. Cavities were not visible in the 5S sample whereas cavity growth was well underway in the 5D sample. As shown in Fig. 6, the 25D and 25SD irradiation produced a strongly bimodal cavity size distribution, but cavities of intermediate size (10-30 nm) were more profuse in the case of 25D irradiation. The cavity size distribution in

20% cold worked specimens (Fig. 7) was not bimodal. At 25 dpa, the 25D specimen contained no cavities larger than 8 nm. The 25SD history produced, in addition to the high number density of small cavities, a very low number density of cavities as large as 14 nm. Although the cavity volume fraction is low in both cases, it is higher for the 25SD specimen, i.e., the lack of helium at low dose seemed to enhance the swelling.

The dependence of the average cavity diameter in the SA, SAA and CW specimens on irradiation dose is shown in Fig. 8. The dependence for large and small cavities on damage level is similar for the three different thermomechanical treatments prior to the irradiation. The average size of the small cavities ($\lesssim$ 3 nm) is independent of the dose. The average diameter of large cavities increases with increasing total dose. The average large cavity size in the 25SD specimens are smaller than that in the 25D specimens. The dependence of the cavity number density on irradiation dose is shown in Fig. 9. The dependence of the number density for large and small cavities is similar for SA, SAA and CW materials. The large cavities have a rather strong dependence on dose without a saturation tendency, and the small cavities have a weak dependence on dose. The number density of small cavities in the 25SD samples are slightly higher than those for the dual-ion irradiated materials, 25D.

The average cavity volume fraction that was computed from the average cavity diameters and cavity number densities in the SA, SAA and CW specimens is shown in Fig. 10. The cavity volume fraction data for SAA specimens that were obtained in this study are in good agreement with the previous data obtained by G. Ayrault et al. [5] The average cavity volume fraction in SA specimens is lower than in SAA specimens because of a lower average cavity diameter of large cavities and a lower number density of large cavities. The

average cavity volume fractions in the 25SD specimens are higher than those in the 25D samples, especially for SA and SAA specimens. The higher number density of large cavities in the 25SD specimens in comparison with the 25D specimens, both in SA and SAA materials, caused the higher cavity volume fraction in the 25SD specimens. These differences appear to have a close relation to the dislocation and precipitate density in these materials.

DISCUSSION

A qualitative summary of the radiation-induced microstructural changes is shown in Tables 2 and 3. In SA and SAA materials, Table 2, helium scheduling effects are very similar to each other, and 25SD samples showed higher swelling at 25 dpa than 25D samples. The origin of this difference in swelling may be (1) a difference in simultaneous helium injection and no helium injection up to 5 dpa or (2) a difference in helium injection rate, i.e., 15 appm He/dpa or 18.8 appm He/dpa from 5 dpa to 25 dpa. As to the effect of helium injection rate, G. Ayrault et al. [5] have determined that the 5 and 15 appm He/dpa irradiations produced similar microstructures and swelling, but irradiation with 50 appm He/dpa produced higher cavity number densities and greater swelling. If we consider the large-cavity number density, large-cavity mean size and cavity volume fraction in light of explanation (2) above, we find that all three quantities for the 25SD samples are, indeed, near to those expected for continuous helium injection with 18.8 appm He/dpa, based on the results in ref. 5. But there may be an overestimation in the expected value based on linear Helium/dpa ratio dependence of microstructure change between 15 to 50 appm He/dpa (from Ayrault's [5] data); and the high dislocation density value in the 25SD samples being higher than that in the 25D samples is very difficult to

understand.

The absence or presence of helium in the initial stage of damage structure nucleation (i.e. explanation 1 above) may be the dominant cause of the helium scheduling effect. We suggest that the helium atoms cause a higher number density of Frank loops with smaller mean loop size than in specimens without helium, giving a higher dislocation density than in specimens without helium. Also helium apparently suppresses the formation of radiation-induced precipitates which are the dominant nucleation site for cavities in this study. The mechanism for suppression of the the formation of radiation-induced precipitates needs to be investigated in more detail, but a high number density of small needle-like precipitates in the 5S samples seems the dominant origin of high swelling value in the 25SD samples. In CW materials, the helium scheduling effect is not significant. In this material, there is a sleight difference in cavity size distribution, with a low density of cavities larger than 10 nm in the 25SD samples which are absent in the 25D samples. This tendency can be understood by a helium effect at the initial stage of damage formation but not by a helium injection rate dependence. The cavity nucleation in the 5D sample may have taken place together with the recovery of dislocations in 20% cold worked material. In the cold worked samples, the initial dislocation density was very high which made it difficult to form large cavities at 25 dpa. On the other hand, in the 5S samples recovery of the dislocation density took place without helium atoms, which caused substantial reduction of dislocation density and no cavity nucleation. As a result, large cavities could be formed on needle-like precipitates in the regions locally free of dislocations.

The difference of prior thermomechanical treatments, i.e., SA and SAA, is also shown in Table 2. The higher swelling values in SAA than in SA is often

attributed to the low carbon concentration in the matrix resulting from carbide precipitation by aging. But this mechanism cannot explain the results obtained here. The present results indicate that the number density of nucleation sites for cavities is much higher in SAA than in SA materials, especially for large cavities. This may indicate that during the initial stage of damage nucleation the SAA samples had many precipitates which could act as cavity nucleation sites and hence the number density of large cavities in SAA is higher than in SA. Therefore, helium scheduling effects seem to come mainly from the initial stage of damage nucleation, and the cavity growth stage seems to be less important than the cavity nucleation stage for the microstructure development at the 25 dpa level.

J. A. Spitznagel et al. [6] have discussed the concept of a critical cavity size for a transition from gas-driven to bias-driven cavity growth, which was suggested from observations of bimodal cavity size distributions in dual-ion irradiated materials by means of a helium "inventory". They showed that experimentally determined maximum equilibrium bubble sizes and "upper bound" theoretical cavity sizes for a transition from gas-driven bubble growth to bias-driven void growth were in reasonable agreement. We used the following equation to calculate the helium concentration in cavities:

$$\alpha = \gamma 8\pi N^{-2}/3(kT + 2B\gamma/\bar{r}) \qquad (1)$$

where α: He concentration in cavities, γ: surface free energy

N: cavity number density, $\bar{r}$: mean cavity radius

k: Boltzman's constant, T: irradiation temperature

B: Van der Waals constant.

The bimodal distribution of cavities was separated into small cavities as bubbles and large cavities as voids. We adopted eq. (1) for bubbles and for voids we put the experimentally determined maximum equilibrium radius, r_c, into $\bar{r}$ in eq. (1) to obtain helium concentrations in cavities. Here, r_c is taken to be the minimum radius separating the small and large cavities in the bimodal distribution. He concentrations in cavities were calculated as shown in Table 4 using the following values for the the parameters

$$\gamma = 1000 \text{ erg/cm}^2, \; T = 625 \text{ C}, \; B = 1.64 \times 10^{-23} \text{cm}^3, \; r_c = 3.75 \text{ nm}.$$

The results for the 25SD samples for SA material show that calculated He values are a great deal higher than the injected helium values. These results suggest that there may be an overestimation in the calculations. Still the results of this calculation may give us some indication about helium partition to cavities. In 5 dpa irradiated samples for SA and SAA materials, helium values were very close to the injected He value. On the other hand, with an additional 20 dpa dual-ion irradiation with 300 appm of helium injection, only about half of the injected He was partitioned to cavities. These results seem to indicate that He trapping at voids is a small effect and pipe diffusion along dislocations is significant. This mechanism may be supported by the results for CW material with 5 dpa dual-ion irradiation. The material contained about half the amount of helium which was calculated for SA and SAA materials with the same irradiation condition. The 25SD samples, especially for SA material, seem to show that the initial 5 dpa single ion irradiation was effective to nucleate bubbles, and the subsequent 20 dpa dual-ion irradiation was dominated by bubble growth and partly by void growth which resulted in the high helium concentration values for cavities. The lower

values of helium partitioned to cavities in SAA and CW than in SA material may be due to the helium partitioned to precipitates and dislocations, respectively.

To get information about cavity growth, we calculated the cavity growth rate using M. R. Hayns and L. K. Mansur's theory [7], where cavity growth rate is the result of growth from vacancy absorption, and shrinkage from interstitial absorption and thermal vacancy emission. This calculation is adapted to void growth and to bubble growth, i.e., for growth of cavities smaller than the critical bubble size, r_c, a He pressure driven growth mechanism with helium atom flow into bubbles was used [8]. The cavity growth rates were calculated from cavity number density values as a function of cavity size. The swelling rate values that were obtained are shown in Table 5. For the 5S samples and the 25SD samples, the lack of information to obtain an experimental swelling rate does not allow present values in Table 5. As far as the 5D and the 25D samples, the calculated values and the experimentally obtained values showed good agreement. These results do not mean that such a simplified calculation can predict cavity growth in dual-ion irradiated 316 SS. However, these results may tell, at least for small cavities and large cavities, whether growth is "pressure-driven cavity growth" or "bias-driven cavity growth", respectively.

CONCLUSIONS

1. In SA and SAA samples, the dislocation density increased rapidly up to about 5 dpa and then gradually increased to a saturation density at 25 dpa. This transition of dislocation density to saturation corresponds to the unfaulting of Frank loops.

2. In CW samples, the dislocation density decreased rapidly up to 5 dpa and then increased slowly to saturation value.
3. Dual-ion irradiation to 25 dpa produced strongly bimodal cavity size distributions in SA and SAA samples, whereas single-ion irradiation followed by dual-ion to 25 dpa produced a cavity size distribution with a substantial component of intermediate size cavities.
4. In 20% cold worked material, dual-ion irradiation produced only very small cavities, while single-ion followed by dual-ion irradiation produced some intermediate size cavities.
5. Needle-like precipitates were induced by radiation which were mainly aligned along <100> directions and were the dominant nucleation sites for cavities.
6. Cavity growth rate and swelling rate were calculated after Hayns and Mansur's theory which could reasonably explain the results obtained for dual-ion irradiated samples.

Differences in microstructures after irradiation that are caused by differences in helium injection schedule are quite complex and surprisingly persistent.

ACKNOWLEDGEMENTS

The authors wish to express their appreciation to B. A. Loomis for helpful discussions.

REFERENCES

[1] A. Taylor, J. Wallace, D. I. Potter, D. G. Ryding and B. O. Hall, "Argonne National Laboratory Dual-Ion Irradiation System", pp. I-158-190 in Radiation Effects and Tritium Technology for Fusion Reactors, J. S. Watson and F. W. Wiffen eds., NTIS, US-DOE, Springfield, VA (1976).

[2] A Kohyama and G. Ayrault, "Carbon Spot Technique for Foil Thickness Measurement of Heavily Irradiated Materials", to be published.

[3] N. Igata, A. Kohyama and K. Itadani, "Radiation Effects on Molybdenum Alloys Bombarded by Electrons in a High-Voltage Electron Microscope", pp. 12-31, in Effects of Radiation on Structural Materials, J. A. Sprague and D. Kramer eds., ASTM STP-683 (1979).

[4] N. Igata, Y. Kohno, M. Saito and H. Tsunakawa "Void Swelling of Modified 316 Stainless Steels Observed In-Situ by HVEM", Journal of Nuclear Materials 103 & 104 (1981) 1047-1052.

[5] G. Ayrault, H. A. Hoff, F. V. Nolfi, Jr., and A. P. L. Turner, "Influence of Helium Injection Rate on the Microstructure of Dual-Ion Irradiated Type 316 Stainless Steel", Journal of Nuclear Materials 103 & 104 (1981) 1035-1040.

[6] J. A. Spitznagel, S. Wood, and W. J. Choyke; DAFS Quarterly Report No. 9, Jan.-Mar. (1980).

[7] M. R. Hayns and L. K. Mansur, "Application of the Theory of Cavity Growth to Dual-Ion Swelling Experiments", in Effects of Radiation on Materials, D. Kramer, H. R. Brager and J. S. Perrin, eds., ASTM STP-725 (1981).

[8] Y. Kohno, A. Kohyama, G. Ayrault, N. Igata and T. Takeyama, "Cavity Growth in Dual-Ion and/or Electron Irradiated Type 316 Stainless Steel", to be published.

Table 1. Irradiation Conditions

	SOLUTION ANNEALED		SOLUTION ANNEALED AND AGED		20% COLD WORKED	
	Temp. (C)	dpa (dpa/sec)	Temp. (C)	dpa dpa/sec)	Temp.(C)	dpa (dpa/sec)
5 dpa Ni-ion	652.7	4.6 (2.7×10^{-3})	637.0	5.0 (2.9×10^{-3})	632.4	4.8 (2.8×10^{-3})
5 dpa dual-ion with 15 appm He/dpa	617.5	4.7 (3.0×10^{-3})	623.1	5.0 (3.1×10^{-3})	624.7	4.8 (3.0×10^{-3})
5 dpa Ni-ion and 20 dpa dual-ion with 15 appm He/dpa*	613.3	23.4 (3.0×10^{-3})	630.2	24.8 (3.2×10^{-3})	620.0	24.1 (3.1×10^{-3})
25 dpa dual-ion with 15 appm He/dpa	617.5	23.5 (3.0×10^{-3})	621.6	24.7 (3.2×10^{-3})	623.1	23.7 (3.1×10^{-3})

* : average He/dpa value

Table. 2. Irradiation Induced Microstructure Change
(qualitative summary)

SOLUTION ANNEALED AND SOLUTION ANNEALED AND AGED TYPE 316 SS

	5 DPA	25 DPA
DISLOCATION	Mainly Frank loop with diameter and number of Frank loops: $d_{FL}(5S) > d_{FL}(5D)$	Mainly tangled dislocations with $\rho_d(25D) \simeq \rho_d(25SD)$ and
	$N_{FL}(50) > N_{FL}(5S) \gg N_{FL}(25D) \simeq N_{FL}(25SD)$	
PRECIPITATES	NEEDLE-LIKE (IRRADIATION INDUCED) PRECIPITATES	
	$\rho_p(5S) > \rho_p(5D)$	$\rho_p(25D) \simeq \rho_p(25SD) > \rho_p(5D)$
	Preferentially oriented. Precipitates in 5D are more highly aligned than those in 5S.	Preferentially oriented.
CAVITY	5S: very close to cavityless 5D: bimodal size distribution Cavities associated with precipitates and Frank loops.	BIMODAL SIZE DISTRIBUTION 25SD has more intermediate size (8-30 nm) cavities than 25D.

DIFFERENCES IN SOLUTION ANNEALED AND SOLUTION ANNEALED AND AGED SAMPLES

1) $d_{FL}(SA) > d_{FL}(SAA)$.
2) $N_{FL}(SA) \simeq N_{FL}(SAA)$.
3) Rather large precipitates that are larger in SAA than in SA.
4) Precipitates show better alignment in SA than in SAA.
5) $d_{cav}(SA) \simeq d_{cav}(SAA)$
6) $N_{cav.large}(SA) < N_{cav.large}(SAA)$
7) Swelling (SA) < Swelling (SAA)

Table 3. Irradiation Induced Microstructure Change
(qualitative summary)

20% COLD WORKED TYPE 316 STAINLESS STEEL

	5 DPA	25 DPA
DISLOCATION	Recovery of dislocations Frank loop fraction is very low	
PRECIPITATE	Smaller needle-like precipitates than those in SA and SAA samples that are not well aligned number density of precipitates is very low $\rho_p(5S) \simeq \rho_p(5D) < \rho_p(25SD) \simeq \rho_p(25D)$	
CAVITY	5S: very close to cavityless 5D: very small in size and very high in number density	uni-modal size distribution larger cavities in 25SD than in 25D

Table 4. Helium Concentration in Cavities (at. ppm)

	Solution Annealed	Solution Annealed and Aged	Cold Worked	He Conc. Injected
5D	60	51	28	75
25SD	657	381	197	375
25D	140	192	169	375

Table 5. Swelling Rate in Dual-Ion Irradiated Type 316 SS

Experimental: 625 C, 3×10^{-3} dpa/sec, 15 appm He/dpa

Theoretical: after M. R. Haynes and L. K. Mansur's theory

	Theoretical	Experimental
5 DPA		
Sol. Ann.	2.6×10^{-2}	1.0×10^{-2}
Sol. Ann. & Age	2.7×10^{-2}	2.2×10^{-2}
Cold Worked	(2.0×10^{-4})	(1.0×10^{-5})
25 DPA		
Sol. Ann.	5.4×10^{-2}	3.4×10^{-2}
Sol. Ann. & Age	7.0×10^{-2}	6.5×10^{-2}
Cold Worked	(2.0×10^{-4})	(5.0×10^{-4})

(%/dpa)

FIGURE CAPTIONS

Fig. 1. Microstructures of solution annealed 316 SS, Ni-ion irradiated at 625°C.

Fig. 2. Microstructures of solution annealed and aged 316 SS, Ni-ion irradiated at 625°C.

Fig. 3. Microstructures of 20% cold worked 316 SS, Ni-ion irradiated at 625°C.

Fig. 4. Dislocation Density in Dual-Ion Irradiated (total density: blank mark, Frank loop density: half filled mark) and Single or Single-plus Dual-Ion Irradiated (total density: filled mark) Type 316 SS.

Fig. 5. Cavity Size Distribution in Solution Annealed Type 316 SS (average cavity diameter: small cavities, open symbol; large cavities, filled symbol).

Fig. 6. Cavity Size Distribution in Solution Annealed and Aged Type 316 SS (average cavity diameter: small cavities, open symbol; large cavities, filled symbol).

Fig. 7. Cavity Size Distribution in 20% Cold-Worked Type 316 SS (open symbol: average cavity diameter.

Fig. 8. The Dependence of Average Cavity Diameter on Irradiation Dose in Dual-Ion Irradiated (blank mark) and Single-plus Dual-Ion Irradiated (filled mark) Type 316 SS.

Fig. 9. The Dependence on Irradiation Dose of Cavity Number Density in Solution Annealed, Solution Annealed and Aged, and 20% Cold Worked Type 316 SS.

Fig. 10. Dependence of the Average Cavity Volume Fraction in SA, SAA, and CW Type 316 SS on Dual Ion (blank mark) or Single plus Dual Ion (filled mark) Irradiation.

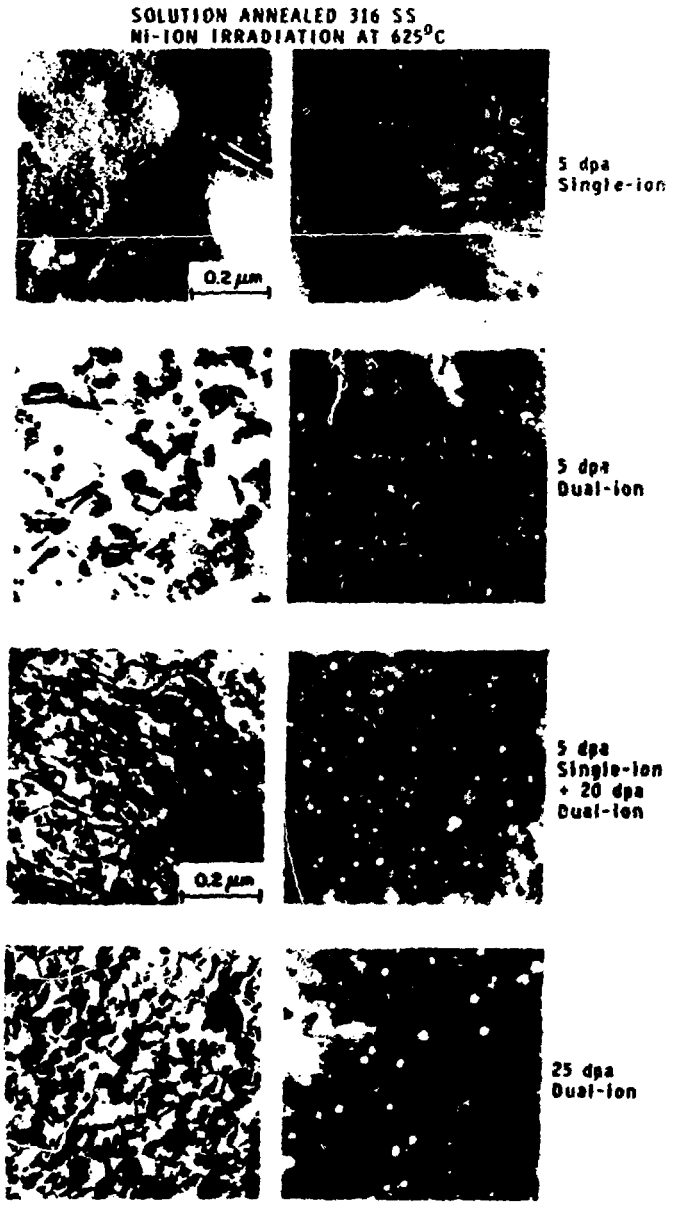

Fig. 1. Microstructures of solution annealed 316 SS, Ni-ion irradiated at 625°C.

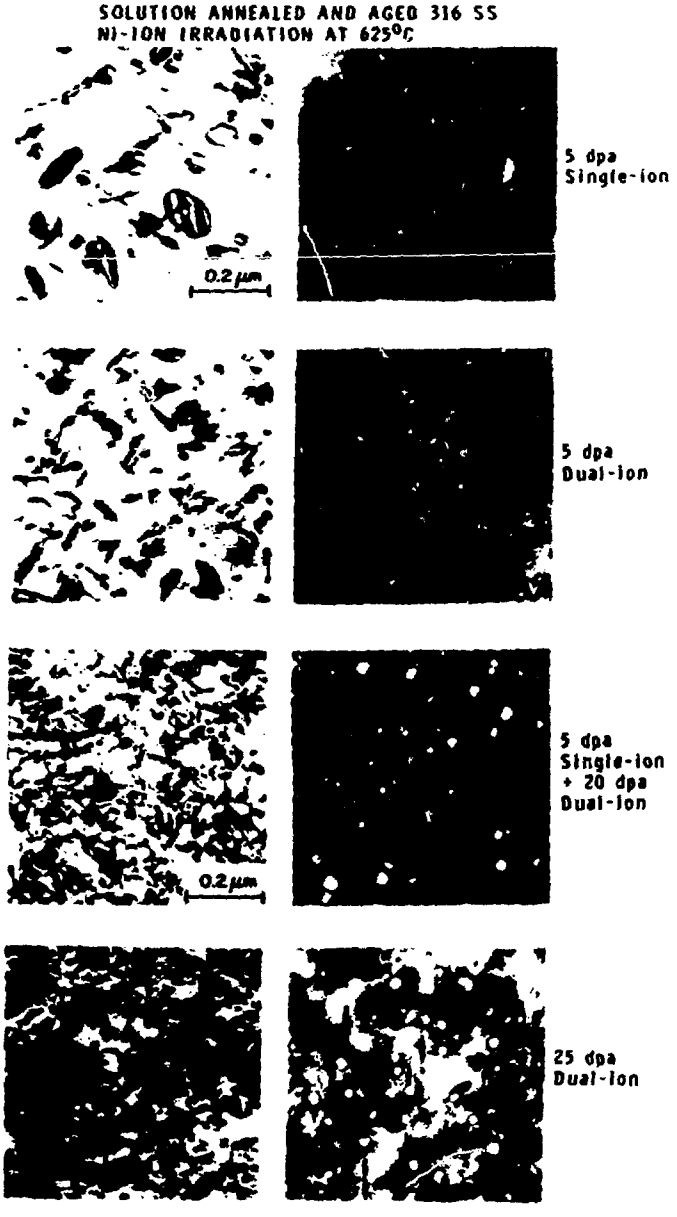

Fig. 2. Microstructures of solution annealed and aged 316 SS, Ni-ion irradiated at 625°C.

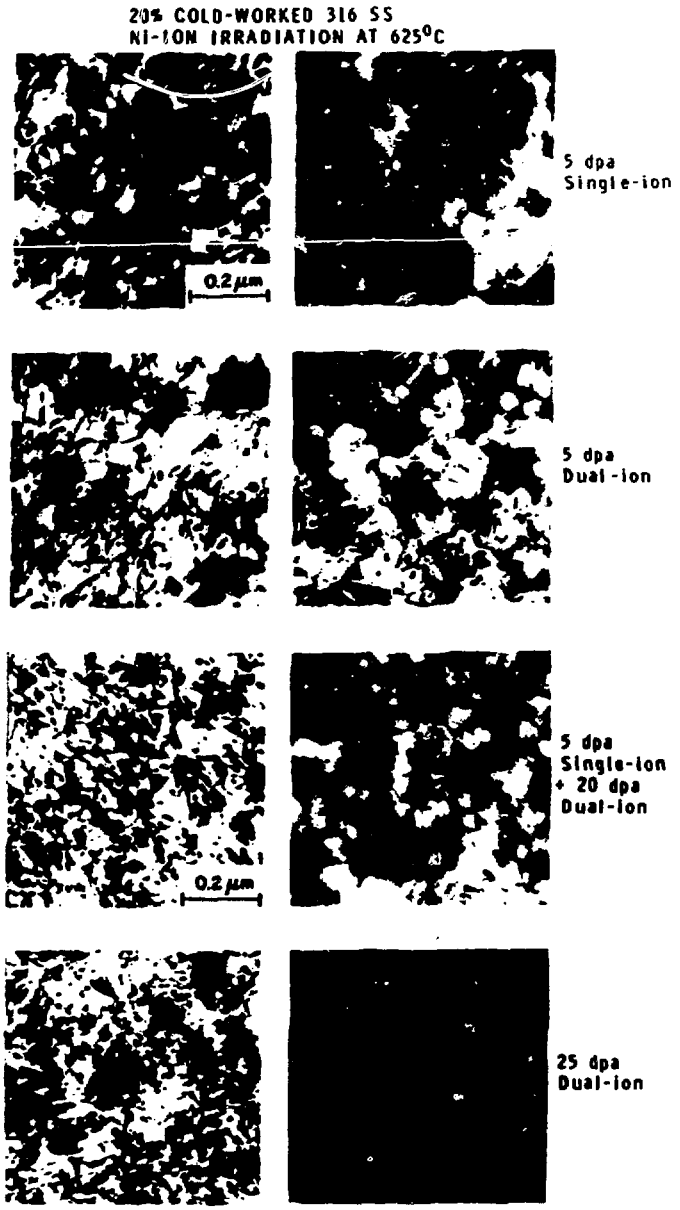

Fig. 3. Microstructures of 20% cold worked 316 SS, Ni-ion irradiated at 625°C.

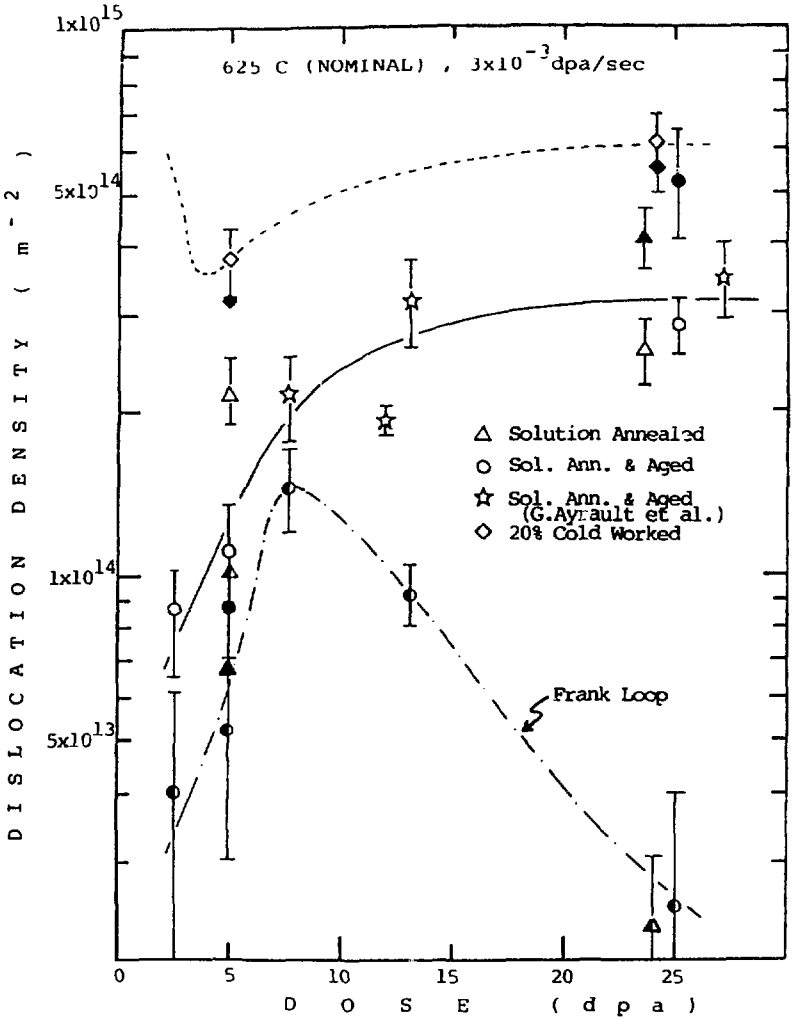

DISLOCATION DENSITY IN DUAL-ION IRRADIATED(total density:blank mark, Frank loop density:half filled mark) AND SINGLE OR SINGLE PLUS DUAL-ION IRRADIATED (total density:filled mark) Type 316 SS

Fig. 4

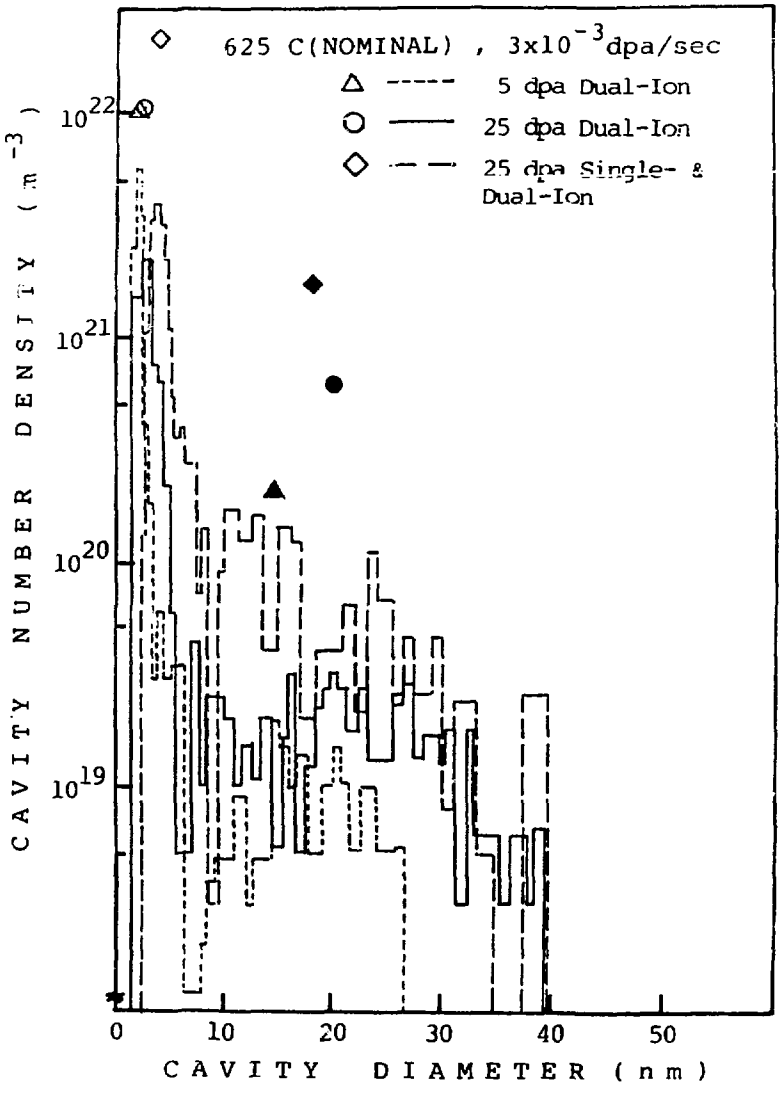

CAVITY SIZE DISTRIBUTION IN SOLUTION ANNEALED Type 316 SS
(average cavity diameter: small cavities, open symbol; large cavities, filled symbol)

Fig. 5

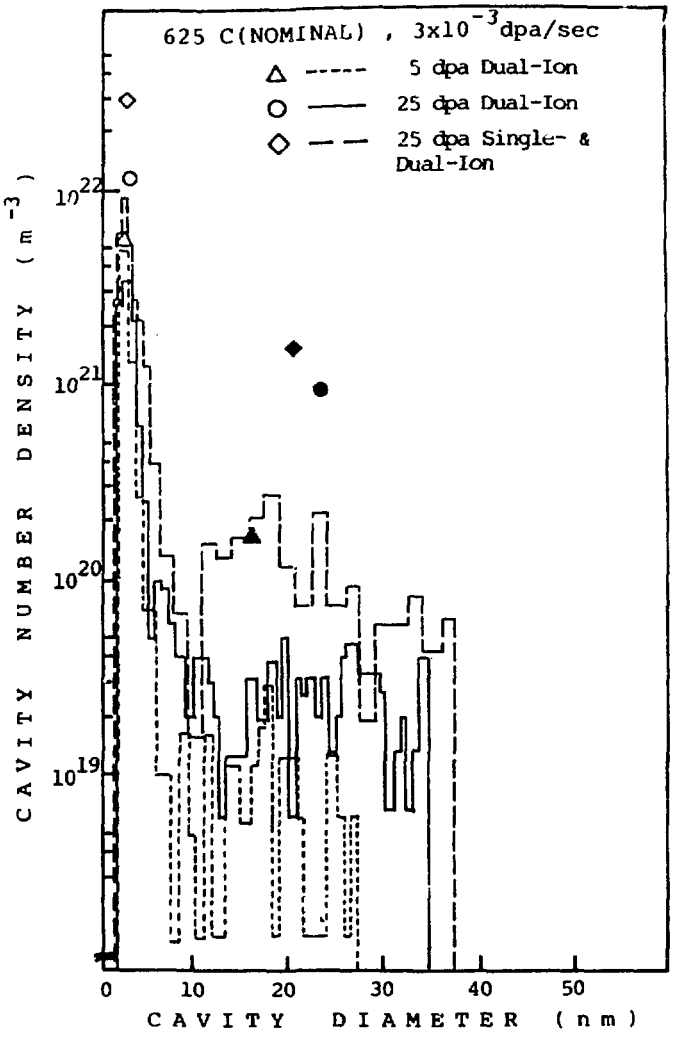

CAVITY SIZE DISTRIBUTION IN SOLUTION ANNEALED AND AGED Type 316 SS
(average cavity diameter: small cavities, open symbol; large cavities, filled symbol)

Fig. 6

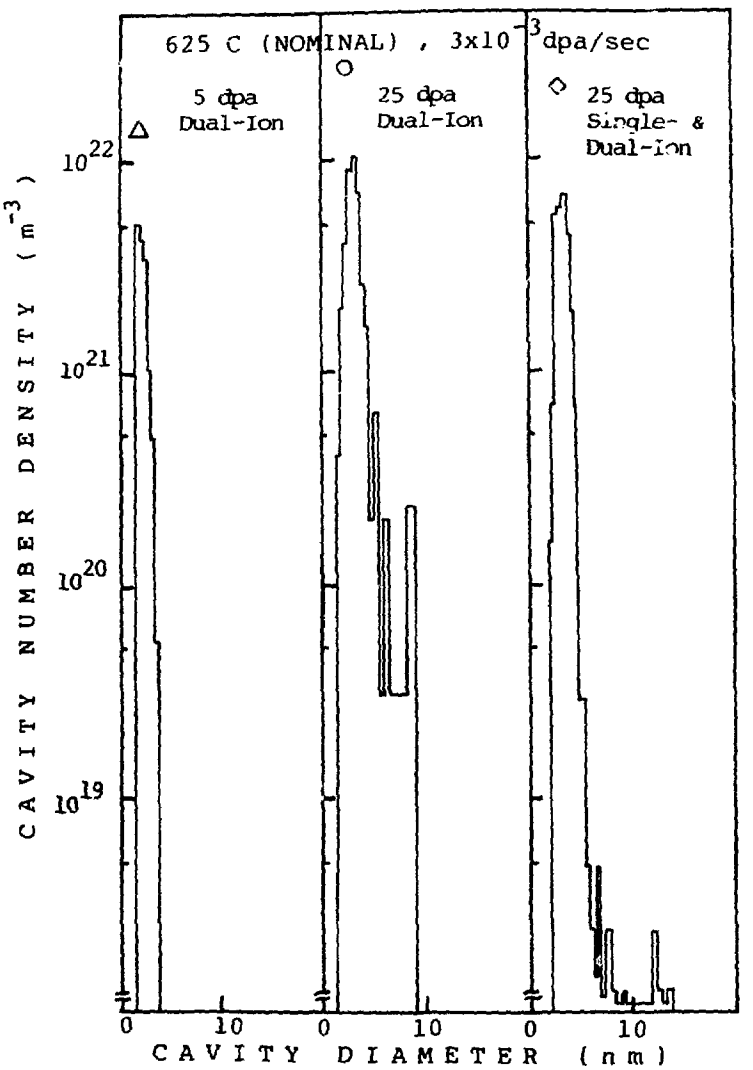

CAVITY SIZE DISTRIBUTION IN 20% COLD WORKED
Type 316 SS
(open symbol:average cavity diameter)

Fig. 7

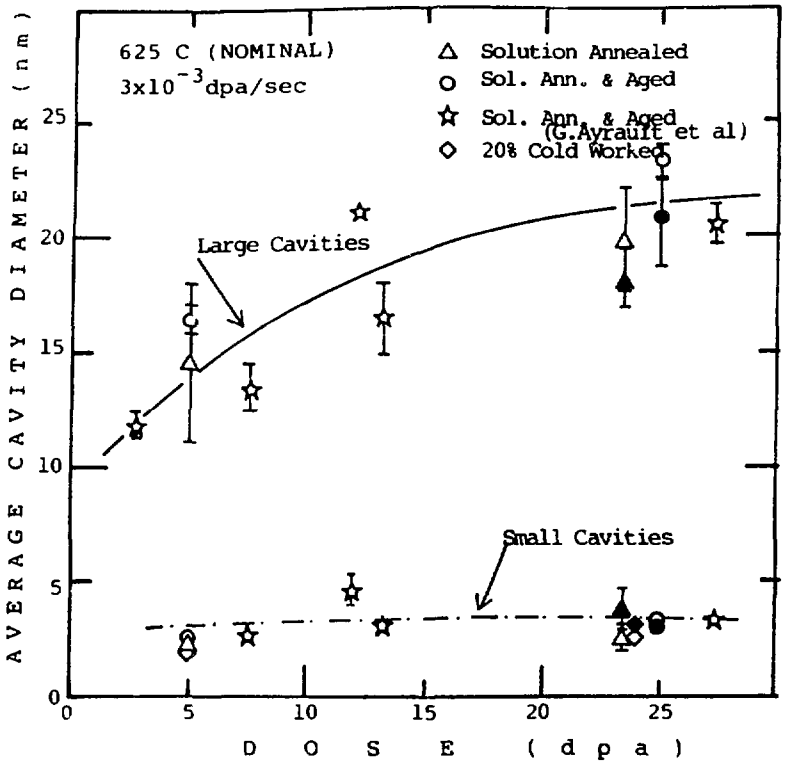

THE DEPENDENCE OF AVERAGE CAVITY DIAMETER ON IRRADIATION DOSE IN DUAL-ION IRRADIATED(blank mark) AND SINGLE- PLUS DUAL-ION IRRADIATED(filled mark) Type 316 SS

Fig. 8

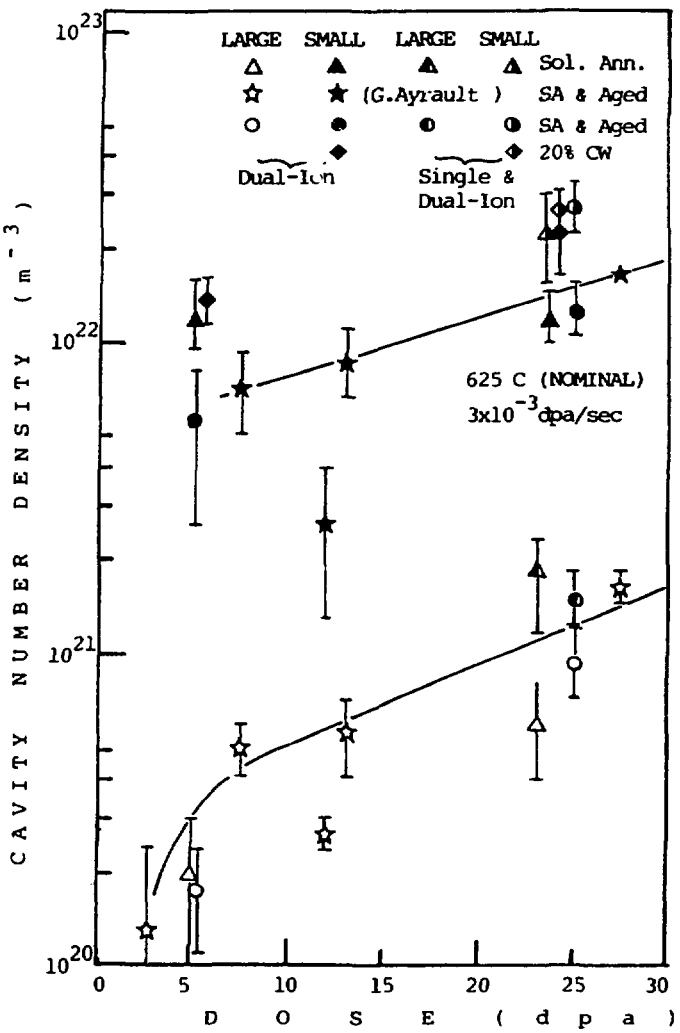

THE DEPENDENCE ON IRRADIATION DOSE OF CAVITY NUMBER DENSITY IN SOLUTION ANNEALED , SOLUTION ANNEALED AND AGED, AND 20% COLD WORKED Type 316 SS

Fig. 9.

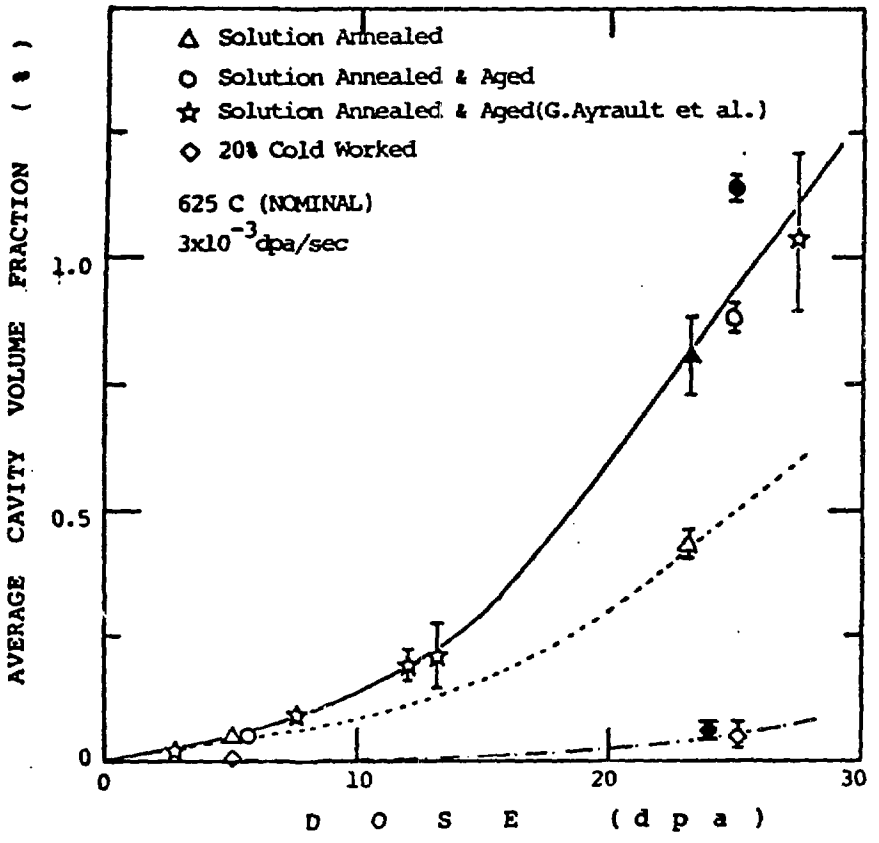

Fig. 10 Dependence of the Average Cavity Volume Fraction in SA, SAA and CW Type 316 SS on Dual Ion (blank mark) or Single Plus Dual Ion (filled mark) Irradiation.